Dinuclear Metal Carbonyls Bridged by Pyridyl Ligands Incorporating an Alkyne Entity

Jiann T. Lin,*,† Shih-Sheng Sun,† Jiann Jung Wu,†,‡ Liangshiu Lee,‡ Kuan-Jiuh Lin,† and Yi Fong Huang†

Institute of Chemistry, Academia Sinica, Nankang, Taipei, Taiwan, Republic of China, and Department of Chemistry, National Sun Yat-Sen University, Kaohsiung, Taiwan, Republic of China

Received November 1, 1994[⊗]

New pyridyl ligands, 1,4-bis(4′-pyridylethynyl)benzene (**1, BPEB**), ferrocenyl-4-pyridylacetylene (**12, FPA**), and (4-nitrophenyl)-4′-pyridylacetylene (**17, NPPA**), which contain an alkyne entity in the backbone, are synthesized. Ligation of these compounds as well as 4,4′-dipyridylbutadiyne (**DPB**) provides $[(OC)_4(L)W]_2(\mu$-**DPB**) (**2**, L = CO; **3**, L = PEt_3; **4**, L = PPh_3; **5**, L = $P(OEt)_3$; **6**, L = $P(OPh)_3$), $[(OC)_4(L)W]_2(\mu$-**BPEB**) (**7**, L = CO; **8**, L = PMe_3; **9**, L = PPh_3; **10**, L = $P(OMe)_3$; **11**, L = $P(OEt)_3$), $W(CO)_4(L)$(**FPA**) (**13**, L = CO; **14**, L = PEt_3; **15**, L = PPh_3; **16**, L = $P(OEt)_3$), and $W(CO)_4(L)$(**NPPA**) (**18**, L = CO; **19**, L = PEt_3; **20**, L = PPh_3; **21**, L = $P(OEt)_3$). The energy of the metal to pyridyl π^* charge-transfer (MLCT) is dependent on both the pyridyl ligand and the ancillary ligand, L. X-ray structural analyses for **6**, **10**, **16**, and **19** were carried out: **6**, $C_{58}H_{38}N_2O_{14}P_2W_2$, orthorhombic, *Pcba*, $Z = 4$, $a = 13.636(3)$ Å, $b = 19.442(5)$ Å, $c = 20.299(7)$ Å, $R = 0.031$, $R_w = 0.029$; **10**, $C_{34}H_{30}N_2O_{14}P_2W_2$, triclinic, $P\bar{1}$, $Z = 1$, $a = 8.428(3)$ Å, $b = 10.996(4)$ Å, $c = 11.894(4)$ Å, $\alpha = 110.68(3)°$, $\beta = 90.28(3)°$, $\gamma = 105.88(3)°$, $R = 0.031°$, $R_w = 0.035$; **16**, $C_{27}H_{28}FeNO_7PW$, orthorhombic, $P2_12_12_1$, $Z = 4$, $a = 9.903(1)$ Å, $b = 14.536(3)$ Å, $c = 20.059(3)$ Å, $R = 0.041$, $R_w = 0.041$; **19**, $C_{23}H_{23}N_2O_6PW$, orthorhombic, *Pcba*, $Z = 8$, $a = 14.178(2)$ Å, $b = 15.007(2)$ Å, $c = 23.878(2)$ Å, $R = 0.033$, $R_w = 0.034$.

Introduction

The alkyne unit is a versatile functional group which undergoes a large number of useful transformations.[1] Juxtaposition of the alkyne entity and ligands appears to be interesting in several aspects: (a) two or more metal centers could be held in the same molecule[2] for cooperative effect in catalysis; (b) metal organic polymers could be derived from organometallic complexes containing these ligands;[3] (c) bridged dinuclear complexes could serve as models for the investigation of metal–metal interactions[4] or the complex may serve as nonlinear optical materials.[5]

Dipyridyl bridging ligands incorporating the alkyne entity have been widely used for the construction of dinuclear complexes.[6] In contrast, to our knowledge, there was no report on dimeric metal carbonyl complexes with such a bridging ligand. We therefore set out to synthesize organometallic complexes of this type. The presence of carbonyl ligands should offer the opportunity for tuning the metal environment electronically and sterically via ligand substitution. Furthermore, the strong metal to ligand charger transfer (MLCT) normally present in pyridyl metal complexes[7] has been suggested to be beneficial for construction of nonlinear optical materials.[8] In this report, we will describe the syntheses and structural and spectroscopic studies of some dinuclear tungsten carbonyl complexes bridged by dipyridyl ligands incorporating the alkyne entity. Related tungsten carbonyls which contain the monopyridyl ligands with alkyne entities are also included.

Experimental Section

General Procedures. All reactions and manipulations were carried out under N_2 with the use of standard inert-atmosphere and Schlenk techniques. Solvents were dried by standard procedures. All column chromatography was performed under N_2 with use of silica gel (230–400 mesh ASTM, Merck) as the stationary phase in a column 35 cm in length and 2.5 cm in diameter. $PdCl_2(PPh_3)_2$,[9] $Pd(PPh_3)_4$,[10] (η^5-IC_5H_4)(η^5-C_5H_5)Fe,[11] $W(CO)_4(L)(THF)$ (L = CO, phosphine),[12] 4-ethynylpyridine,[13] 4,4′-dipyridylbutadiyne (**DPB**),[13] 1,4-diethynylbenzene,[14] and anhydrous $ZnCl_2$[15] were prepared by published procedures. Infrared measurements were measured on a Perkin-Elmer 880 spectrometer. The

* To whom correspondence should be addressed. Telefax: 886-2-7831237. e-mail: jtlin@chem.sinica.edu.tw.

† Academia Sinica.

‡ National Sun Yat-Sen University.

⊗ Abstract published in *Advance ACS Abstracts,* April 1, 1995.

(1) Patai, S., Ed. *The Chemistry of the Carbon-Carbon Triple Bond*; Wiley-Interscience: Chichester, U.K., 1978.

(2) (a) Bunz, U. H. F.; Enkelmann, V.; Räder, J. *Organometallics* **1993**, *12*, 4745. (b) Wiegelmann, J. E. C.; Bunz, U. H. F. *Organometallics* **1993**, *12*, 3792. (c) Sterzo, C. L.; Stille, J. K. *Organometallics* **1990**, *9*, 687. (d) Sterzo, C. L.; Miller, M. M.; Stille, J. K. *Organometallics* **1989**, *8*, 2331.

(3) (a) Jia, G.; Puddephatt, R. J.; Vittal, J. J.; Payne, N. C. *Organometallics* **1993**, *12*, 263. (b) Zeldih, M.; Wynne, K.; Allcock, H. R. Eds. *Inorganic and Organometallic Polymers*; Advances in Chemistry Series 224; American Chemical Society: Washington DC, 1988.

(4) Bunel, E. E.; Valle, L.; Jones, N. L.; Carroll, P. J.; Gonzalez, M.; Munoz, N.; Manriquez, J. M. *Organometallics* **1988**, *7*, 789.

(5) (a) Yuan, Z.; Stringer, G.; Jobe, I. R.; Kreller, D. *J. Organomet. Chem.* **1993**, *452*, 115.

(6) (a) Grosshenny, V.; Ziessel, R. *J. Chem. Soc., Dalton Trans.* **1993**, 817. (b) Das, A.; Maher, J. P.; McCleverty, J. A.; Badiola, J. A. N.; Ward, M. D. *J. Chem. Soc., Dalton Trans.* **1993**, 681. (c) Potts, K. T.; Horwitz, C. P.; Fessak, A.; Keshararz, K. M.; Nash, K. E.; Toscano, P. J. *J. Am. Chem. Soc.* **1993**, *115*, 10444. (d) Sutton, J. E.; Taube, H. *Inorg. Chem.* **1981**, *20*, 3125.

(7) Geoffroy, G. L.; Wrighton, M. S. Eds. *Organometallic Photochemistry*; Academic Press: New York 1979.

(8) (a) Kanis, D. R.; Ratner, M. A.; Marks, T. J. *Chem. Rev.* **1994**, *94*, 195. (b) Bourgault, M.; Tam, W.; Eaton, D. F. *Organometallics* **1990**, *9*, 2856.

(9) Colquhoun, H. M.; Holton, J.; Thompson, D. J.; Twigg, M. V. Eds. *New Pathways for Organic Synthesis*; Plenum Press: New York, 1984; Chapter 9.

(10) Coolson, D. R. *Inorg. Synth.* **1972**, *13*, 122.

(11) Jones, K.; Lappert, M. F. *J. Organomet. Chem.* **1965**, *3*, 295.

(12) (a) Kolodziej, R. M.; Lees, A. J. *Organometallics* **1986**, *5*, 450. (b) Bancroft, R. T.; Arndt, L. W.; Delord, T.; Darensbourg, M. Y. *J. Am. Chem. Soc.* **1986**, *108*, 2617.

(13) Ciana, L. D.; Haim, A. *J. Heterocycl. Chem.* **1984**, *21*, 607.

(14) Austin, W. B.; Bilow, N.; Kelleghan, W. J.; Lau, K. S. Y. *J. Org. Chem.* **1981**, *46*, 2280.

(15) Perrin, D. D.; Armarego, W. L. F.; Perrin, D. R. Eds. *Purification of Laboratory Chemicals*, 2nd ed.; Pergamon Press: Oxford, U.K., 1980.

0020-1669/95/1334-2323$09.00/0

NMR spectra were measured by using Bruker AMX500 (^{1}H, ^{31}P), AC200 (^{1}H), and AC300 (^{1}H, ^{31}P) spectrometers. Electronic absorption spectra was obtained on a Perkin-Elmer Lambda 9 spectrometer. Electrochemical measurements were recorded on a Bioanalytical Systems BAS 100B. Cyclic voltammograms were obtained in deoxygenated dry CH_2Cl_2 with a platinum working electrode, a platinum-wire auxiliary electrode, and a saturated $Ag/AgNO_3$ reference electrode with 0.1 M tetrabutylammonium perchlorate (TBAP) as supporting electrolyte. In some cases ferrocene, which was known to undergo a discrete one-electron transfer process, was added and used as internal reference for both of potential calibration and for reversibility criteria. In CH_2Cl_2 the ferrocene has $E_{1/2}$ at 0.223 V relative to Ag/Ag^+ and the anodic peak-cathodic peak separation is 105 mV. All E_P values for the complexes in this study are reported relative to ferrocene (i.e., 0.00 V for ferrocene). The concentration of the metal carbonyl complexes in these measurements was $\sim 10^{-3}$ M. The scan rate was 80 mV s^{-1}. The measurements were uncorrected for liquid-junction potentials. Elemental analyses were performed on a Perkin-Elmer 2400 CHN analyzer.

1,4-Bis(4′-pyridylethynyl)benzene (BPEB, 1). Et_2NH (70 mL) was added to a flask containing a mixture of 4-bromopyridine hydrochloride (4.74 g, 24.0 mmol), 1,4-diethynylbenzene (1.5 g, 12.0 mmol), $Pd(PPh_3)_2Cl_2$ (420 mg, 1.0 mmol), and CuI (114 mg, 1.0 mmol). The resulting mixture was heated at 60−65 °C for 48 h. The solvent was removed in vacuo and the residue was extracted with Et_2O to provide yellow-orange powdery **1** (2.7 g, 81%). ^{1}H NMR (acetone-d_6): δ 8.64 (d, 4 H, $^3J_{H-H}$ = 5.8 Hz), 7.66 (s, 4 H), 7.48 (d, 4 H, $^3J_{H-H}$ = 5.8 Hz). MS (FAB): *m/e* 281 $(M + 1)^+$. Anal. Calcd for $C_{20}H_{12}N_2$: C, 85.69; H, 4.31; N, 9.99. Found: C, 85.30; H, 4.21; N, 9.75.

$(OC)_4(L)W(\mu$-DPB)$W(CO)_4(L)$ (2, L = CO; 3, L = PEt_3; 4, L = PPh_3; 5, L = $P(OEt)_3$; 6, L = $P(OPh)_3$) and $(OC)_4(L)W(\mu$-BPEB)$W(CO)_4(L)$ (7, L = CO; 8, L = PMe_3; 9, L = PPh_3; 10, L = $P(OMe)_3$; 11, L = $P(OEt)_3$). For the syntheses of **2**−**11**, essentially the same procedures were followed, and only the preparation of **4** will be described in detail. A THF solution of $W(CO)_4(PPh_3)(THF)$ prepared in situ from $W(CO)_6$ (1.0 g, 2.84 mmol) and PPh_3 (0.75 g, 2.84 mmol) was reduced in volume to 100 mL and transferred to a flask containing **DPB** (0.30 g, 1.50 mmol). The solution was stirred for 18 h, and the solvent was removed under vacuum. The residue was dissolved in CH_2Cl_2 and soaked with 2 g of silica and pumped dry. It was then carefully placed on the top of the column packed with silica/hexane and chromatographed under nitrogen. Elution with CH_2Cl_2/hexane (1:3) gave an deep red band from which powdery **4** was isolated in 31% yield (1.16 g) after removal of solvent. MS (FAB): 1318 (M^+, ^{184}W). Anal. Calcd for $C_{58}H_{38}N_2O_8P_2W_2$: C, 52.74; H, 2.90; N, 2.12. Found: C, 52.62; H, 2.86; N, 2.02.

Orange complex **2** was eluted with CH_2Cl_2/hexane (1:3) and had a yield of 30%. MS (FAB): *m/e* 852 (M^+, ^{184}W). Anal. Calcd for $C_{22}H_8N_2O_{10}W_2$: C, 33.83; H, 0.95; N, 3.08. Found: C, 34.21; H, 1.09; N, 2.91.

Purple complex **3** was eluted with CH_2Cl_2/hexane (2:3) and had a yield of 35%. MS (FAB): *m/e* 1030 $((M + 1)^+$, ^{182}W). Anal. Calcd for $C_{34}H_{38}N_2O_8P_2W_2$: C, 39.55; H, 3.71; N, 2.71. Found: C, 39.02; H, 3.50; N, 2.52. Further elution with CH_2Cl_2/hexane (2:1) gave complex $(CO)_4(PEt_3)W(\eta^1$-**DPB**) in low yield. IR (CH_2Cl_2, cm^{-1}): 2009 m, 1978 vs, 1840 s. ^{1}H NMR (acetone-d_6): δ 9.08 (d, 2 H, $^3J_{H-H}$ = 6.7 Hz, NC*H*), 8.67 (d, 2 H, $^3J_{H-H}$ = 6.7 Hz, NCHC*H*), 7.54 (d, 2 H, $^3J_{H-H}$ = 4.8 Hz, NC*H*), 7.53 (d, 2 H, $^3J_{H-H}$ = 4.8 Hz, NCHC*H*), 1.78 (quint, 6 H, $^2J_{H-P}$ = 7.5 Hz, $^3J_{H-H}$ = 7.5 Hz, CH_2), 1.02 (td, 9 H, $^3J_{H-H}$ = 7.5 Hz, $^3J_{H-P}$ = 11.7 Hz, CH_3); ^{31}P NMR (acetone-d_6): δ 12.3 (s, J_{P-W} = 226 Hz).

Deep red complex **5** was eluted with CH_2Cl_2/hexane (2:3) and had a yield of 32%. MS (FAB): *m/e* 1158 (M^+, ^{184}W). Anal. Calcd for $C_{34}H_{38}N_2O_{14}P_2W_2$: C, 36.19; H, 3.39; N, 2.28. Found: C, 35.78; H, 3.56; N, 2.21.

Red complex **6** was eluted with CH_2Cl_2/hexane (1:2) and had a yield of 28%. MS (FAB): *m/e* 1416 (M^+, ^{186}W). Anal. Calcd for $C_{58}H_{38}N_2O_{14}P_2W_2$: C, 49.17; H, 2.70; N, 1.98. Found: C, 48.90; H, 2.51; N, 1.84.

Orange yellow complex **7** was eluted with CH_2Cl_2/hexane (3:2) and had a yield of 33%. MS (FAB): *m/e* 928 (M^+, ^{184}W). Anal. Calcd for $C_{30}H_{12}N_2O_{10}W_2$: C, 38.82; H, 1.30; N, 3.02. Found: C, 38.97; H, 1.19; N, 3.06.

Deep red complex **8** was eluted with CH_2Cl_2/hexane (1:2) and had a yield of 28%. MS (FAB): *m/e* 1024 (M^+, ^{184}W). Anal. Calcd for $C_{34}H_{30}N_2O_8P_2W_2$: C, 39.90; H, 3.00; N, 2.70. Found: C, 39.62; H, 2.80; N, 2.51.

Orange complex **9** was eluted with CH_2Cl_2/hexane (2:3) and had a yield of 25%. MS (FAB): *m/e* 1396 (M^+, ^{184}W). Anal. Calcd for $C_{64}H_{42}N_2O_8P_2W_2$: C, 55.00; H, 3.00; N, 2.00. Found: C, 55.23; H, 3.08; N, 2.21.

Orange red complex **10** was eluted with CH_2Cl_2/hexane (2:3) and had a yield of 32%. MS (FAB): *m/e* 1119 $((M + 1)^+$, ^{184}W). Anal. Calcd for $C_{34}H_{30}N_2O_{14}P_2W_2$: C, 36.45; H, 2.70; N, 2.51. Found: C, 36.61; H, 2.51; N, 2.40.

Dark red complex **11** was eluted with CH_2Cl_2/hexane (2:3) and had a yield of 23%. MS (FAB): *m/e* 1206 (M^+, ^{186}W). Anal. Calcd for $C_{40}H_{42}N_2O_{14}P_2W_2$: C, 39.89; H, 3.51; N, 2.32. Found: C, 40.37; H, 3.51; N, 2.22.

Ferrocenyl-4-pyridylacetylene (FPA, 12). To a flask containing a mixture of 1-iodoferrocene (0.60 g, 1.93 mmol), 4-((trimethylstannyl)-ethynyl)pyridine (0.50 g, 1.88 mmol), and $Pd(PPh_3)_4$ (150 mg, 0.13 mmol) was added 75 mL of THF, and the solution was heated at 45−50 °C for 24 h. The solvent was removed in vacuum, and the residue was extracted with Et_2O/H_2O. The Et_2O layer was transfer to a flask containing $MgSO_4$ to remove H_2O and filtered. The filtrate was pumped dry and the residue was chromatographed. Elution with CH_2Cl_2/hexane (1:1) afforded two bands. The first band was the unreacted 1-iodoferrocene. Removal of the solvent from the second band provided red powdery **12** in 74% yield (400 mg). ^{1}H NMR (acetone-d_6): δ 8.55 (d, 2 H, $^3J_{H-H}$ = 6.1 Hz), 7.37 (d, 2 H, $^3J_{H-H}$ = 6.1 Hz), 4.57 (t, $^3J_{H-H}$ = 1.8 Hz, 2 H), 4.35 (t, $^3J_{H-H}$ = 1.8 Hz, 2 H), 4.26 (s, 5 H). MS (FAB): *m/e* 310 (M^+). Anal. Calcd for $C_{17}H_{13}NFe$: C, 71.10; H, 4.60; N, 4.90. Found: C, 70.937; H, 4.43; N, 4.75.

$W(CO)_4(L)$(FPA) (13, L = CO; 14, L = PEt_3; 15, L = PPh_3; 16, L = $P(OEt)_3$). Complexes **13**−**16** were synthesized by the same procedures as for the syntheses of **4** except that **FPA** was used instead of **DPB**.

Brick red complex **13** was eluted with CH_2Cl_2/hexane (1:4) and had a yield of 30%. MS (FAB): *m/e* 611 (M^+, ^{184}W). Anal. Calcd for $C_{22}H_{13}NO_5FeW$: C, 43.24; H, 2.14; N, 2.29. Found: C, 43.20; H, 1.89; N, 2.15.

Orange red complex **14** was eluted with CH_2Cl_2/hexane (1:4) and had a yield of 24%. Anal. Calcd for $C_{27}H_{24}NO_4PFeW$: C, 46.25; H, 4.02; N, 2.00. Found: C, 45.90; H, 3.57; N, 1.85.

Orange complex **15** was eluted with CH_2Cl_2/hexane (3:2) and had a yield of 34%. MS (FAB): *m/e* 846 $((M + 1)^+$, ^{184}W). Anal. Calcd for $C_{39}H_{28}NO_4PFeW$: C, 49.50; H, 3.34; N, 1.66. Found: C, 49.83; H, 2.97; N, 1.56.

Orange red complex **16** was eluted with CH_2Cl_2/hexane (1:4) and had a yield of 28%. MS (FAB): *m/e* 750 $((M + 1)^+$,^{184}W). Anal. Calcd for $C_{27}H_{28}NO_7PFeW$: C, 43.29; H, 3.76; N, 1.87. Found: C, 43.44; H, 3.42; N, 1.75.

(4-Nitrophenyl)-4′-pyridylacetylene (NPPA, 17). A 11.2 mL of *t*-BuLi (1.6 M in THF, 19.0 mmol) was added in a period of 10 min to a THF solution of 4-ethynylpyridine (1.94 g, 18.8 mmol) prechilled to −70 °C. After 45 min the color of the solution was light purple, and a THF solution of $ZnCl_2$ (2.56 g, 18.8 mmol) was added. The solution was allowed to warm to room temperature ane stirred for another 1 h. The reaction solution was then added to 4-iodonitrobenzene (4.69 g, 18.8 mmol) and $Pd(PPh_3)_4$ (550 mg, 0.48 mmol). After 18 h the solution was pumped dry and the residue was extracted with Et_2O. Removal of Et_2O provided 3.72 g (81% yield) of yellow powdery **17**. ^{1}H NMR (acetone-d_6): δ 8.66 (d, 2 H, $^3J_{H-H}$ = 6.2 Hz), 8.31 (d, 2 H, $^3J_{H-H}$ = 9.0 Hz), 7.87 (d, 2 H, $^3J_{H-H}$ = 9.0 Hz), 7.52 (d, 2 H, $^3J_{H-H}$ = 6.2 Hz). MS (FAB): *m/e* 225 $(M + 1)^+$. Anal. Calcd for $C_{13}H_8N_2O_2$: C, 69.64; H, 3.60; N, 12.49. Found: C, 69.50; H, 3.33; N, 12.31.

$W(CO)_4(L)$(NPPA) (18, L = CO; 19, L = PEt_3; 20, L = PPh_3; 21, L = $P(OEt)_3$). Complexes **18**−**21** were synthesized by the same procedures as for the syntheses of **4** except that **NPPA** was used instead of **DPB**.

Table 1. Crystal Data for Compounds **6**, **10**, **16**, and **19**

	6	**10**	**16**[c]	**19**
chem formula	$C_{58}H_{38}N_2O_{14}P_2W_2$	$C_{34}H_{30}N_2O_{14}P_2W_2$	$C_{27}H_{28}FeNO_7PW$	$C_{23}H_{23}N_2O_6PW$
f_w	1416.59	1120.25	749.18	638.27
space group	*Pcba*	$P\bar{1}$	$P2_12_12_1$	*Pcab*
a, Å	13.636(3)	8.428(3)	9.903(1)	14.178(2)
b, Å	19.422(5)	10.996(4)	14.536(3)	15.007(2)
c, Å	20.299(7)	11.894(4)	20.059(3)	23.878(2)
α, deg		110.68(3)		
β, deg		90.28(3)		
γ, deg		105.88(3)		
V, Å^3	5376(3)	985.6(6)	2887.6(8)	5080(1)
Z	4	1	4	8
T, °C	+25	+25	+25	+25
λ(Mo Kα), Å	0.7107	0.7107	0.7107	0.7107
ϱ_{calc}, g cm^{-3}	1.750	1.888	1.723	1.669
μ, cm^{-1}	89.9	121.2	92.0	47.4
transm coeff	1.00−0.90	1.00−0.51	1.00−0.67	1.00−0.81
R[a]	0.031	0.031	0.037	0.033
R_w[b]	0.029	0.035	0.038	0.034

[a] $R = \sum||F_o| - |F_c||/\sum|F_o|$. [b] $R_w = [\sum w(|F_o| - |F_c|)^2/\sum w|F_o|^2]^{1/2}$; $w = 1/[\sigma^2(F_o) + kF_o^2]$. For **6**, $k = 0.00004$; for **10**, **16**, and **19**, k = 0.0001. [c] Chirality $\eta = 0.95(6)$, indicating that the crystal was of a single structure polarity.

Yellow orange complex **18** was eluted with CH_2Cl_2/hexane (1:5) and had a yield of 35%. Anal. Calcd for $C_{18}H_8N_2O_7W$: C, 39.45; H, 1.47; N, 5.11. Found: C, 39.65; H, 1.55; N, 5.11.

Dark purple complex **19** was eluted with CH_2Cl_2/hexane (2:3) and had a yield of 30%. MS (FAB): *m/e* 638 (M^+, ^{184}W). Anal. Calcd for $C_{23}H_{23}N_2O_6PW$: C, 43.28; H, 3.63; N, 4.39. Found: C, 43.29; H, 3.50; N, 4.27.

Dark purple complex **20** was eluted with CH_2Cl_2/hexane (2:3) and had a yield of 34%. MS (FAB): *m/e* 783 ($(M + 1)^+$, ^{184}W). Anal. Calcd for $C_{35}H_{23}N_2O_6PW$: C, 53.17; H, 2.96; N, 3.58. Found: C, 53.09; H, 2.57; N, 3.43.

Dark purple complex **21** was eluted with CH_2Cl_2/hexane (1:1) and had a yield of 41%. MS (FAB): *m/e* 687 (M^+ ^{184}W). Anal. Calcd for $C_{23}H_{23}N_2O_9PW$: C, 40.25; H, 3.37; N, 4.08. Found: C, 40.57; H, 2.96; N, 4.03.

(4-Aminophenyl)-4′-pyridylacetylene (APPA, 22). Pale yellow complex **22** was synthesized by the same procedures as for the synthesis of **17** except that 4-iodoaniline was used instead of 4-iodonitrobenzene. It was isolated in 74% yield. ^1H NMR (acetone-d_6): δ 8.53 (d, 2 H, $^3J_{H-H} = 5.2$ Hz, NC*H*), 7.35 (d, 2 H, $^3J_{H-H} = 5.2$ Hz, NCHC*H*), 7.28 (d, 2 H, $^3J_{H-H} = 8.4$ Hz, C*H*CHNH$_2$), 6.69 (d, 2 H, $^3J_{H-H} = 8.4$ Hz, CHC*H*NH$_2$), 5.14 (s, 2 H, N*H*$_2$). MS (FAB): *m/e* 194 (M^+). Anal. Calcd for $C_{13}H_{10}N_2$: C, 80.39; H, 5.19; N, 14.42. Found: C, 79.10

W(CO)$_5$(APPA) (23). Complex **23** was synthesized by the same procedures as for the syntheses of **4** except that **APPA** was used instead of **DPB**. Dark purple complex **23** was eluted with CH_2Cl_2/hexane (2:3) and had a yield of 49%. IR (CH_2Cl_2, cm^{-1}): 2016 (w), 1958 (vw), 1927 (s), 1895 (sh), ν(CO). ^1H NMR (acetone-d_6): δ 8.92 (d, 2 H, $^3J_{H-H} = 6.6$ Hz, NC*H*), 7.45 (d, 2 H, NCHC*H*), 7.32 (d, 2 H, $^3J_{H-H} = 8.6$ Hz, C*H*CHNH$_2$), 6.71 (d, 2 H, CHC*H*NH$_2$), 5.29 (s, 2H, N*H*$_2$). MS (FAB): *m/e* 518 (M^+, ^{184}W). Anal. Calcd for $C_{18}H_{10}N_2O_5W$: C, 41.73; H, 1.95; N, 5.41. Found: C, 41.60; H, 1.80; N, 5.34.

Crystallographic Studies. Crystals of **6** were grown by slow diffusion of hexane into a concentrated solution of complex **6** in THF, and crystals of **10**, **16**, and **19** were grown by slow diffusion of hexane into a concentrated solution of relevant complexes in CH_2Cl_2. Crystals were mounted in thin-walled glass capillaries. Diffraction measurements were made on an Enraf-Nonius CAD4 diffractometer by using graphite-monochromated Mo Kα radiation ($\lambda = 0.7107$ Å) with the $\theta-2\theta$ scan mode. Unit cells were determined by centering 25 reflections in the suitable 2θ range. Other relevant experimental details are listed in Table 1. All data reduction and refinements were carried out on MicroVax 3800 computer using NRCVAX[16] programs. Intensities were collected and corrected for decay, absorption (empirical, ψ-scan) and *Lp* effects. Each structure was solved by direct methods[17] and refined on *F* by using full-matrix least-squares techniques. An *E*-map from the starting set with the highest combined figure of merit revealed coordinates for W and Fe atoms. The remaining non-H atoms were located from successive difference Fourier maps. All nonhydrogen atoms were refined anisotropically. All hydrogen atoms were included in the structure factor calculation in idealized positions with $d_{C-H} = 0.95$ Å. The final positional parameters are listed in Table 2, and selected interatomic distances and bond angles are given in Table 3.

(16) Gabe, E. J.; LePage, Y.; Charland, J. P.; Lee, F. L.; White, P. S. *J. Appl. Crystallogr.* **1989**, *22*, 384.

Results and Discussion

The coupling reaction[18] between 1,4-diethynylbenzene and 4-bromopyridine catalyzed by 4−5 mol % of $PdCl_2(PPh_3)_2$ and 4−5 mol % of CuI in diethylamine gives 1,4-bis(4′-pyridylethynyl)benzene (**BPEB**, **1**) in good yield. Symmetrically bridged dimer compounds, (OC)$_4$(L)W(μ-**DPB**)W(CO)$_4$(L) (**2**, L = CO; **3**, L = PEt_3; **4**, L = PPh_3; **5**, L = P(OEt)$_3$; **6**, L = P(OPh)$_3$) and (OC)$_4$(L)W(μ-**BPEB**)W(CO)$_4$(L) (**7**, L = CO; **8**, L = PMe_3; **9**, L = PPh_3; **10**, L = P(OMe)$_3$; **11**, L = P(OEt)$_3$), were synthesized by reacting **DPB** (4,4′-dipyridylbutadiyne) (eq 1) or **BPEB** (eq 2) with W(CO)$_4$(L)(THF)[12] prepared in situ

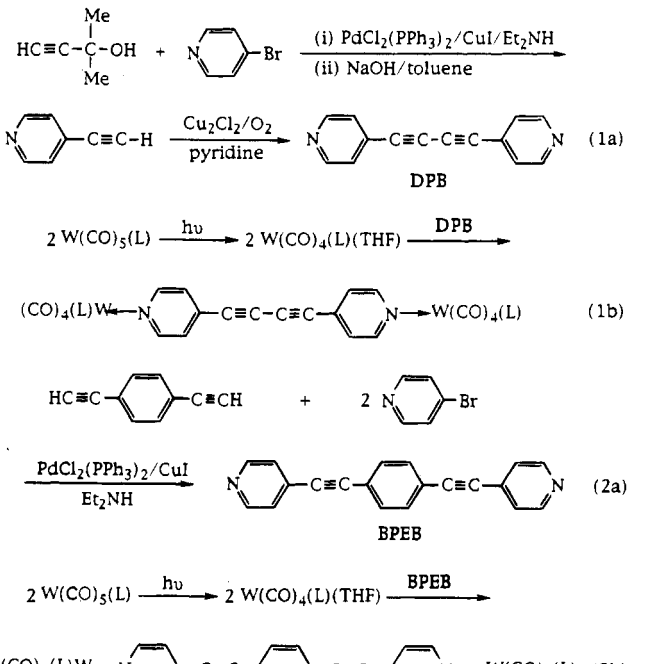

from photolysis of W(CO)$_5$(L). Chromatographic workup is necessary to ensure the purity of these complexes. Although there is nonnegligible decomposition during chromatography, complexes **2**−**11** are moderately stable as solids. The yields for **2**−**11** are comparable or only slightly better than those reported for analogous homonuclear dimers containing a dipyridyl bridge.[19] Palladium(0)-catalyzed Stille coupling[20] using 4-pyridyl(trimethylstannyl)acetylene and 1-iodoferrocene produces 4-ferrocenyl-4-pyridylacetylene (**FPA**, **12**) in 74% yield. Coordination of the dangling pyridine of **12** to W(CO)$_4$)(L)-(THF) leads to the formation of heteronuclear dimers, W(CO)$_4$-

(17) Mai, P.; Fiske, S. J.; Hull, S. E.; Lessinger, L.; Germain, G.; Declercq, J. P.; Woolfson, M. M. Multan82.

(18) (a) Takahashi, S.; Kuroyama, Y.; Sonogashira, K.; Hagihara, N. *Synthesis* **1980**, 627. (b) Sonogashira, K.; Tohda, Y.; Hagihara, N. *Tetrahedron Lett.* **1975**, 4467.

(19) Gaus, P. L.; Buncella, J. M.; Rosengren, K. S.; Funk, M. O. *Inorg. Chem.* **1982**, *21*, 2174.

(20) For review: Stille, J. K. *Angew. Chem., Int. Ed. Engl.* **1986**, *25*, 508.

Table 2. Positional Parameters and B_{iso} Values for the Atoms in Compounds **6**, **10**, **16**, and **19**

atom	*x*	*y*	*z*	B_{iso}, Å^2	atom	*x*	*y*	*z*	B_{iso}, Å^2
				Compound **6**					
W	0.31085(3)	0.736107(20)	0.225845(19)	3.247(19)	C11	0.0189(8)	0.5196(6)	0.4757(5)	3.6(5)
P	0.32119(23)	0.63799(14)	0.15137(13)	3.44(13)	C21	0.1960(9)	0.5706(5)	0.0706(5)	3.7(5)
O1	0.2950(7)	0.8577(5)	0.3279(4)	7.2(5)	C22	0.1166(8)	0.5892(6)	0.0338(5)	4.2(6)
O2	0.5148(6)	0.7025(4)	0.2940(4)	6.1(5)	C23	0.0906(10)	0.5499(7)	−0.0202(6)	6.0(8)
O3	0.4337(7)	0.8369(5)	0.1400(4)	7.1(5)	C24	0.1417(11)	0.4890(8)	−0.0340(7)	6.2(8)
O4	0.1311(7)	0.7868(5)	0.1415(4)	7.2(5)	C25	0.2205(10)	0.4731(6)	0.0048(7)	5.8(7)
O5	0.2151(5)	0.6141(3)	0.1251(3)	3.7(4)	C26	0.2461(9)	0.5113(6)	0.0582(6)	4.4(6)
O6	0.3865(5)	0.6412(3)	0.0856(3)	3.8(3)	C31	0.3864(9)	0.6949(6)	0.0392(5)	3.8(6)
O7	0.3586(5)	0.5637(3)	0.1782(3)	4.2(4)	C32	0.3039(10)	0.7292(6)	0.0234(5)	4.8(6)
N	0.2189(6)	0.6675(4)	0.2933(4)	3.3(5)	C33	0.3061(12)	0.7805(6)	−0.0249(6)	6.0(7)
C1	0.2996(10)	0.8128(6)	0.2911(6)	4.9(6)	C34	0.3944(14)	0.7935(8)	−0.0556(7)	7.1(9)
C2	0.4381(9)	0.7120(5)	0.2698(6)	4.3(6)	C35	0.4766(11)	0.7596(8)	−0.0381(6)	6.6(8)
C3	0.3891(9)	0.7963(6)	0.1710(5)	4.7(6)	C36	0.4754(8)	0.7101(6)	0.0107(5)	4.5(6)
C4	0.1929(10)	0.7657(6)	0.1746(5)	4.2(5)	C41	0.4445(9)	0.5547(5)	0.2133(5)	3.8(6)
C5	0.1254(8)	0.6490(5)	0.2809(5)	3.8(5)	C42	0.5340(10)	0.5723(5)	0.1866(6)	4.7(7)
C6	0.0671(8)	0.6128(6)	0.3231(5)	4.3(6)	C43	0.6200(9)	0.5587(6)	0.2221(7)	5.7(7)
C7	0.1052(8)	0.5931(5)	0.3836(5)	3.4(5)	C44	0.6104(11)	0.5283(7)	0.2840(7)	6.3(8)
C8	0.2013(9)	0.6114(6)	0.3968(5)	4.7(6)	C45	0.5234(12)	0.5101(7)	0.3074(7)	6.3(8)
C9	0.2541(8)	0.6479(5)	0.3511(5)	4.1(6)	C46	0.4377(10)	0.5230(6)	0.2739(6)	5.1(6)
C10	0.0523(9)	0.5532(6)	0.4319(5)	4.2(6)					
				Compound **10**					
W	0.22165(5)	0.62505(4)	0.33153(4)	3.593(21)	C5	−0.1688(12)	0.5025(11)	0.3233(8)	4.7(6)
P	0.1631(3)	0.8038(3)	0.27160(24)	4.27(15)	C6	−0.3276(12)	0.4225(11)	0.2839(9)	4.9(6)
O1	0.2793(10)	0.3859(8)	0.3970(7)	6.4(5)	C7	−0.3697(12)	0.3299(10)	0.1667(9)	4.1(6)
O2	0.1545(10)	0.7681(8)	0.5977(7)	6.8(5)	C8	−0.2403(13)	0.3277(11)	0.0928(9)	5.0(6)
O3	0.5914(11)	0.7830(10)	0.4296(9)	9.3(6)	C9	−0.0845(12)	0.4107(10)	0.1402(9)	4.4(6)
O4	0.3837(11)	0.5313(9)	0.0893(8)	8.3(6)	C10	−0.5347(13)	0.2427(11)	0.1215(9)	4.7(6)
O5	0.0187(9)	0.7611(8)	0.1672(6)	6.2(5)	C11	−0.6697(13)	0.1706(11)	0.0862(9)	4.8(6)
O6	0.1260(9)	0.9205(7)	0.3835(6)	5.9(5)	C12	−0.8372(12)	0.0833(10)	0.0416(9)	4.2(6)
O7	0.2948(10)	0.8811(8)	0.2077(6)	6.0(5)	C13	−0.9671(14)	0.1113(10)	0.1038(9)	5.1(6)
N	−0.0425(9)	0.4997(8)	0.2568(7)	3.7(4)	C14	−0.8731(13)	−0.0305(11)	−0.0632(10)	5.2(6)
C1	0.2535(12)	0.4728(11)	0.3746(8)	4.2(6)	C15	−0.1481(16)	0.7332(14)	0.1787(12)	7.7(9)
C2	0.1686(13)	0.7125(10)	0.4982(9)	4.6(6)	C16	0.0941(18)	1.0384(13)	0.3674(12)	8.7(10)
C3	0.4458(16)	0.7228(13)	0.3938(10)	6.0(8)	C17	0.4596(17)	0.9509(14)	0.2623(14)	9.2(11)
C4	0.3150(13)	0.5602(11)	0.1731(10)	4.8(6)					
				Compound **16**					
W	0.32628(7)	0.42489(4)	0.13206(3)	2.99(3)	C9	0.6177(16)	0.4320(15)	0.1989(8)	3.6(8)
Fe	1.1607(7)	0.23777(15)	0.41375(10)	3.31(11)	C10	0.8123(18)	0.3620(12)	0.3482(8)	3.8(8)
P	0.3277(6)	0.2561(3)	0.11840(21)	4.01(22)	C11	0.9077(16)	0.3521(12)	0.3823(8)	3.4(8)
N1	0.4896(14)	0.4046(11)	0.2102(7)	3.6(7)	C12	1.0284(18)	0.3436(12)	0.4191(8)	3.2(8)
O1	0.3212(23)	0.6380(9)	0.1606(7)	7.3(9)	C13	1.0472(19)	0.3031(13)	0.4832(8)	4.0(9)
O2	0.0723(14)	0.4078(15)	0.2260(7)	7.8(10)	C14	1.1828(23)	0.3087(13)	0.5010(8)	4.6(10)
O3	0.1188(14)	0.4489(11)	0.0179(6)	6.0(8)	C15	1.2559(18)	0.3546(12)	0.4477(11)	4.6(10)
O4	0.5297(15)	0.4573(11)	0.0114(7)	6.1(8)	C16	1.1580(20)	0.3766(11)	0.3963(8)	4.0(8)
O5	0.1971(19)	0.2110(9)	0.1480(9)	7.9(10)	C17	1.0817(25)	0.1419(21)	0.3536(15)	7.5(15)
O6	0.4471(21)	0.2063(10)	0.1567(10)	9.6(11)	C18	1.098(3)	0.1069(19)	0.4147(16)	6.6(15)
O7	0.3301(24)	0.2101(10)	0.0489(6)	8.8(10)	C19	1.230(4)	0.1086(16)	0.4267(15)	8.1(18)
C1	0.3193(23)	0.5564(13)	0.1508(8)	4.6(9)	C20	1.302(3)	0.1504(15)	0.3744(18)	7.7(15)
C2	0.1675(23)	0.4105(18)	0.1953(8)	4.6(10)	C21	1.198(3)	0.1748(17)	0.3262(11)	7.6(15)
C3	0.1907(23)	0.4396(16)	0.0607(9)	4.2(10)	C22	0.147(3)	0.1227(17)	0.1416(13)	8.8(16)
C4	0.4609(20)	0.4419(15)	0.0570(9)	4.0(10)	C23	0.0123(24)	0.1124(18)	0.1618(12)	7.7(14)
C5	0.4703(17)	0.3641(13)	0.2701(9)	4.4(9)	C24	0.501(4)	0.132(3)	0.156(3)	21.1(42)
C6	0.5697(18)	0.3492(14)	0.3154(9)	4.3(9)	C25	0.611(4)	0.1039(15)	0.1584(14)	11.8(27)
C7	0.7008(17)	0.3761(12)	0.3029(8)	3.7(8)	C26	0.337(5)	0.2336(19)	−0.0101(14)	13.9(27)
C8	0.7214(15)	0.4163(15)	0.2422(8)	4.1(9)	C27	0.316(4)	0.1755(16)	−0.0653(11)	9.5(17)
				Compound **19**					
W	0.49199(3)	0.62316(4)	0.141340(22)	4.57(3)	C8	0.7370(9)	0.4611(9)	0.0786(6)	5.4(7)
P	0.5477(3)	0.6431(3)	0.24117(16)	6.31(22)	C9	0.8156(8)	0.5130(10)	0.0878(6)	4.6(7)
O1	0.4154(8)	0.5990(9)	0.0212(5)	9.7(8)	C10	0.9113(9)	0.4801(10)	0.0734(6)	5.9(8)
O2	0.5436(8)	0.8240(7)	0.1155(5)	8.7(7)	C11	0.9850(9)	0.4533(10)	0.0631(5)	5.8(7)
O3	0.2866(7)	0.6858(8)	0.1658(6)	11.2(8)	C12	1.0795(10)	0.4202(11)	0.0554(7)	5.9(8)
O4	0.4143(9)	0.4364(8)	0.1800(6)	11.1(9)	C13	1.1572(10)	0.4673(10)	0.0710(6)	5.7(8)
O5	1.4170(9)	0.3531(12)	0.0533(8)	16.6(14)	C14	1.0889(9)	0.3365(11)	0.0322(6)	6.0(8)
O6	1.3550(11)	0.2427(11)	0.0110(8)	14.0(13)	C15	1.2462(10)	0.4322(11)	0.0629(7)	6.7(9)
N1	0.6386(7)	0.5729(7)	0.1168(4)	4.7(6)	C16	1.1778(11)	0.3006(10)	0.0249(7)	7.1(10)
N2	1.3506(11)	0.3119(12)	0.0352(9)	9.3(11)	C17	1.2547(10)	0.3511(10)	0.0404(7)	5.7(8)
C1	0.4500(10)	0.6079(11)	0.0672(8)	7.5(10)	C18	0.6470(23)	0.5764(20)	0.2659(9)	22.8(24)
C2	0.5275(9)	0.7504(11)	0.1248(5)	5.6(7)	C19	0.6628(19)	0.4942(17)	0.2571(10)	15.9(18)
C3	0.3649(11)	0.6636(10)	0.1585(6)	7.3(9)	C20	0.5861(12)	0.7552(13)	0.2593(6)	9.1(11)
C4	0.4476(9)	0.5021(11)	0.1656(7)	6.9(9)	C21	0.6168(17)	0.7713(16)	0.3208(7)	14.9(16)
C5	0.7151(9)	0.6240(10)	0.1229(6)	6.0(8)	C22	0.4631(19)	0.6226(20)	0.2960(8)	17.7(21)
C6	0.6501(8)	0.4935(10)	0.0941(6)	5.5(8)	C23	0.3795(16)	0.680(3)	0.2947(12)	28.3(44)
C7	0.8033(9)	0.5954(9)	0.1092(6)	5.6(8)					

(L)(**FPA**) (**13**, L = CO; **14**, L = PEt_3; **15**, L = PPh_3; **16**, L = $P(OEt)_3$) (eq 3). Palladium(0)-catalyzed coupling of organiczinc

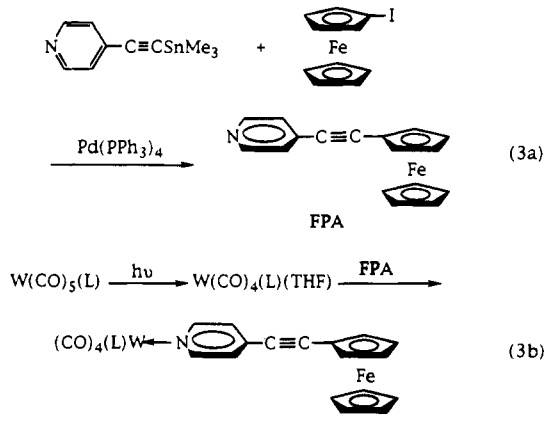

(3a)

(3b)

with aryl halide[21] was successfully applied to the syntheses of (4-nitrophenyl)-4′-pyridylacetylene (**NPPA**, **17**) and (4-aminophenyl)-4′-pyridylacetylene (**APPA**, **22**). These compounds have an organic donor (aminobenzene) or acceptor (nitrobenzene) linked to pyridine through an alkyne. Monomeric complexes $(OC)_4(L)W$(**NPPA**) (**19**, L = PEt_3; **20**, L = PPh_3; **21**, L = $P(OEt)_3$) and $(OC)_5W$(**APPA**) (**23**) were synthesized via the ligation of pyridine (eq 4).

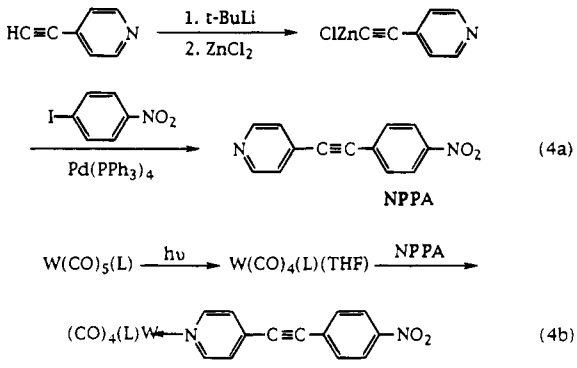

(4a)

(4b)

The spectroscopic properties (Table 4) of these new complexes are consistent with their formulation. The three moderate/strong carbonyl stretching bands for **2**, **7**, **13**, **18**, and **23** in the infrared spectra are characteristic of C_{4v} arrangement of the carbonyl ligands at the metal center, and the three moderate/strong bands for **3**–**6**, **8**–**11**, **14**–**16**, **19**–**21**, **17**, and **19** require that phosphorus donor ligand and pyridine be mutually cis at the tungsten center. The carbonyl stretching frequencies decrease as the π-accepting ability of phosphine ligands increases. However, the difference in pyridine ligands does not seem to affect the carbonyl stretching frequencies to a noticeable degree. Except for triphenylphosphine-substituted complexes, **4**, **9**, **15**, and **20**, the chemical shifts for the α-ring protons of pyridine in the ^1H NMR spectra shift to lower field than those of free ligands (**DPB**, 8.67; **BPEB**, 8.64; **FPA**, 8.55; **NPPA**, 8.66 ppm; **APPA**, 8.53) by 0.3–0.4 ppm upon coordination. The lower δ values for the α-ring protons of pyridine in **4**, **9**, **15**, and **20** is most likely owing to the ring current shielding caused by the phenyl ring of the triphenylphosphine. The ^{31}P NMR spectra of the new complexes contain one signal for the coordinated phosphine, which is accompanied by a pair of tungsten satellites, with $^1J_{P-W}$ = 233–413 Hz. Phosphite-substituted complexes have much higher values of $^1J_{P-W}$, consistent with the trend described by Schenk.[22]

Table 3. Selected Bond Distances (Å) and Angles (deg) for Complexes **6**, **10**, **16**, and **19**

	6	**10**	**16**	**19**
		Distances		
W–P	2.437(3)	2.477(3)	2.469(4)	2.529(4)
W–N	2.285(8)	2.255(7)		
W–N1			2.27(1)	2.29(1)
W–C1	2.00(1)	2.00(1)	1.95(2)	1.88(2)
W–C2	2.01(2)	1.99(1)	2.03(2)	2.01(2)
W–C3	1.94(1)	1.89(1)	1.98(2)	1.94(2)
W–C4	2.00(2)	2.01(1)	2.02(2)	2.01(2)
Fe–C12			2.02(2)	
Fe–C13			2.03(2)	
Fe–C14			2.04(2)	
Fe–C15			2.06(2)	
Fe–C16			2.05(2)	
Fe–C17			2.00(2)	
Fe–C18			2.00(3)	
Fe–C19			2.02(2)	
Fe–C20			2.05(2)	
Fe–C21			2.01(2)	
C1–O1	1.15(2)	1.15(1)	1.20(2)	1.21(2)
C2–O2	1.17(2)	1.15(1)	1.13(3)	1.15(2)
C3–O3	1.18(2)	1.22(2)	1.12(2)	1.17(2)
C4–O4	1.15(2)	1.15(1)	1.17(2)	1.15(2)
N–C5	1.35(1)	1.33(1)		
N–C9	1.32(1)	1.36(1)		
N1–C5			1.35(2)	1.34(2)
N1–C6				1.32(2)
N1–C9			1.35(2)	
C10–C11	1.19(1)	1.17(2)	1.18(2)	1.14(2)
C11–C11a	1.35(2)			
N2–O5				1.21(2)
N2–O6				1.19(2)
		Angles		
C1–W–C2	86.9(5)	89.9(4)	87.3(9)	90.6(6)
C1–W–C3	88.5(5)	88.3(4)	90.6(9)	86.8(6)
C1–W–C4	93.9(4)	91.9(4)	92.7(9)	93.6(7)
C1–W–P	176.6(3)	176.1(3)	174.9(5)	179.7(5)
C1–W–N	89.7(4)	89.2(3)		
C1–W–N1			91.1(7)	90.4(5)
C2–W–C3	85.4(5)	85.9(4)	86.4(8)	88.7(6)
C2–W–C4	173.7(4)	170.0(4)	170.6(7)	173.1(6)
C2–W–P	92.5(3)	90.7(3)	88.3(7)	89.7(4)
C2–W–N	94.1(4)	95.0(4)		
C2–W–N1			96.1(6)	92.0(4)
C3–W–C4	88.3(5)	84.3(4)	84.2(8)	86.0(6)
C3–W–P	94.8(3)	95.6(3)	91.8(7)	93.1(5)
C3–W–N	178.2(4)	177.3(4)		
C3–W–N1			177.0(7)	177.0(5)
C4–W–P	87.1(3)	88.2(3)	92.0(6)	86.2(5)
C4–W–N	92.2(4)	94.9(4)		
C4–W–N1			93.2(6)	93.5(5)
W–C1–O1	178(1)	176.5(8)	177(2)	175(1)
W–C2–O2	175.2(9)	173.2(9)	173(2)	177(1)
W–C3–O3	175(1)	177.6(9)	176(2)	176(1)
W–C4–O4	173(1)	173(1)	173(20	174(1)
P–W–N	87.0(2)	87.0(2)		
P–W–N1			86.8(4)	89.8(3)
C7–C10–C11	172(1)			
O5–N2–O6				126(2)

Electronic Absorption Spectra. Table 5 illustrates the electronic absorption spectra of all new complexes in different solvents at room temperature. The spectra of $(CO)_4(PEt_3)W$-(η^1-**DPB**) and $W(CO)_4(PPh_3)$(piperidine)[23] are also included for comparison. Based on the spectra of free pyridyl ligands, the fairly intense bands at λ < 335 nm are assigned as pipi* pyridyl ligand transition. Similar to many analogous $W(CO)_6$ derivatized mononuclear and dinuclear complexes,[24] metal to π*

(21) (a) Erdik, E. *Tetrahedron* **1992**, *48*, 9577. (b) Negishi, E.; Luo, F. T.; Frisbee, R.; Matsushita, H. *Heterocycles* **1982**, *18*, 117.

(22) Schenk, W. A.; Buchner, W. *Inorg. Chim. Acta* **1983**, *70*, 189.

(23) Darensbourg, D. J.; Kump, R. L. *Inorg. Chem.* **1978**, *17*, 2680.

Table 4. IR Spectra in the ν(CO) Region and ^{1}H and ^{31}P{H} NMR Spectra of Compounds

compd	ν(CO) and ν(C≡C),[a] cm^{-1}	δ, ppm[b,c] (J, Hz)	δ, ppm[b,d] (J, Hz)
2	2072 m, 1975 vw, 1929 s, 1899 sh	9.11(d, 4 H, J_{H-H} = 6.5), 7.66 (d, 4 H, J_{H-H} = 6.5)	
3	2005 m, 1875 vs, 1839 s	9.09 (d, 4 H, J_{H-H} = 6.7, NC*H*), 7.55 (d, 4 H, J_{H-H} = 6.7, NCHC*H*), 1.78 (quint, 12 H, J_{H-H} = 7.2, CH_2), 1.02 (quint, 18 H, J_{H-H} = 7.2, CH_3)	12.3 (s, J_{P-W} = 232)
4	2010 m, 1885 vs, 1857 s	8.60 (d, 4 H, J_{H-H} = 6.4, NC*H*), 7.48−7.39 (m, 30 H, Ph), 7.18 (d, 4 H, J_{H-H} = 6.4, NCHC*H*)	37.2 (s, J_{P-W} = 239)
5	2017 m, 1887 vs, 1854 s	9.03 (d, 4 H, J_{H-H} = 6.5, NC*H*), 7.57 (d, 4 H, J_{H-H} = 6.5, NCHC*H*), 3.98 (m, 12 H, CH_2), 1.22 (m, 18 H, CH_3)	146 (s, J_{P-W} = 380)
6	2026 m, 1902 vs, 1879 s	8.81 (d, 4 H, J_{H-H} = 6.4, NC*H*), 7.46 (d, 4 H, J_{H-H} = 6.4, NCHC*H*), 7.35−7.23 (m, 30 H, Ph)	138 (s, J_{P-W} = 413)
7	2072 m, 1976 vw, 1927 s, 1898 sh	9.06 (d, 4 H, J_{H-H} = 6.9, NC*H*), 7.73 (s, 4 H, Ph), 7.61 (d, 4 H, J_{H-H} = 6.9, NCHC*H*)	
8	2006 m, 1877 vs, 1844 s	9.02 (d, 4 H, J_{H-H} = 6.5, NC*H*). 7.71 (s, 4 H, Ph), 7.52 (d, 4 H, J_{H-H} = 6.5, NCHC*H*), 1.48 (d, 18 H, J_{P-H} = 7.5, CH_3)	−21.7 (s, J_{P-W} = 233)
9	2012 m, 1882 vs, 1846 s	8.57 (d, 4 H, J_{H-H} = 6.3, NC*H*), 7.69 (s, 4 H, Ph), 7.48−7.39 (m, 30 H, PPh_3), 7.16 (d, 4 H, J_{H-H} = 6.3, NCHC*H*)	36.8 (s, J_{P-W} = 245)
10	2020 m, 1891 vs, 1856 s	8.99 (d, 4 H, J_{H-H} = 6.7, NC*H*), 7.72 (s, 4 H, Ph), 7.52 (d, 4 H, J_{H-H} = 6.7, NCHC*H*), 3.60 (d, 18 H, J_{P-H} = 11.1, OCH_3)	152 (s, J_{P-W} = 390)
11	2017 m, 1887 vs, 1853 s	8.99 (d, 4 H, J_{H-H} = 6.7, NC*H*), 7.71 (s, 4 H, Ph), 7.52 (d, 4 H, J_{H-H} = 6.7, NCHC*H*), 3.96 (m, 12 H, CH_2), 1.22 (m, 18 H, CH_3)	147 (s, J_{P-W} = 384)
13	2071 m, 1960 vw, 1928 s, 1880 sh, 2205 w	8.95 (d, 2 H, J_{H-H} = 6.2, NC*H*), 7.48 (d, 2 H, J_{H-H} = 6.2, NCHC*H*), 4.62 (t, 2 H, J_{H-H} = 1.8, C_5H_4), 4.42 (t, 2 H, J_{H-H} = 1.8, C_5H_4), 4.28 (s, 5 H, Cp)	
14	2005 m, 1875 vs, 1839 s, 2207 w	8.93 (d, 2 H, J_{H-H} = 6.7, NC*H*), 7.40 (d, 2 H, J_{H-H} = 6.7, NCHC*H*), 4.60 (t, 2 H, J_{H-H} = 1.8, C_5H_4), 4.41 (t, 2 H, J_{H-H} = 1.8, C_5H_4), 4.28 (s, 5 H, Cp), 1.78 (m, 6 H, CH_2), 1.03 (m, 9 H, CH_3)	12.3 (s, J_{P-W} = 225)
15	2011 m, 1886 vs, 1841 s, 2231 w	8.47 (d, 2 H, J_{H-H} = 6.8, NC*H*), 7.47−7.40 (m, 15 H, Ph), 7.34 (d, 2 H, J_{H-H} = 6.8, NCHC*H*), 4.60 (t, 2 H, J_{H-H} = 1.8, C_5H_4), 4.41 (t, 2 H, J_{H-H} = 1.8, C_5H_4), 4.28 (s, 5 H, Cp)	36.6 (s, J_{P-W} = 245)
16	2017 m, 1886 vs, 1850 s, 2208 m	8.89 (d, 2 H, J_{H-H} = 6.5, NC*H*), 7.40 (d, 2 H, J_{H-H} = 6.5, NCHC*H*), 4.61 (t, 2 H, J_{H-H} = 1.8, C_5H_4), 4.41 (t, 2 H, J_{H-H} = 1.8, C_5H_4), 4.28 (s, 5 H, Cp), 3.98(quint, 6 H, J_{H-P} = 1.8, J_{H-H} = 1.8, CH_2), 1.23 (t, 9 H, J_{H-H} = 1.8, CH_3)	147 (s, J_{P-W} = 382)
18	2072 m, 1960 vw, 1930 s, 1895 sh	9.10 (d, 2 H, J_{H-H} = 6.8, NC*H*), 8.34 (d, 2 H, J_{H-H} = 8.6, C*H*CNO_2), 7.92 (d, 2 H, J_{H-H} = 8.6, C*H*CHCNO_2), 7.66 (d, 2 H, J_{H-H} = 6.8, NCHC*H*)	
19	2006 m, 1874 vs, 1842 s	9.07 (d, 2 H, J_{H-H} = 6.6, NC*H*), 8.33 (d, 2 H, J_{H-H} = 8.6, C*H*CNO_2), 7.90 (d, 2 H, J_{H-H} = 8.6, C*H*CHCNO_2), 7.56 (d, 2 H, J_{H-H} = 6.6, NCHC*H*), 1.79 (m, 6 H, CH_2), 1.03 (m, 9 H, CH_3)	12.3 (s, J_{P-W} = 236)
20	2011 m, 1884 vs, 1849 s	8.59 (d, 2 H, J_{H-H} = 6.8, NC*H*), 8.32 (d, 2 H, J_{H-H} = 8.8, C*H*NO_2), 7.89 (d, 2 H, J_{H-H} = 8.8, C*H*CHCNO_2), 7.48−7.20 (m, 15 H, PPh_3), 7.20 (d, 2 H, J_{H-H} = 6.8, NCHC*H*)	36.9 (s, J_{P-W} = 244)
21	2017 m, 1886 vs, 1854 s	9.02 (d, 2 H, J_{H-H} = 6.6, NC*H*), 8.33 (d, 2 H, J_{H-H} = 9.0, C*H*CNO_2), 7.91 (d, 2 H, J_{H-H} = 9.0, C*H*CHCNO_2), 7.57 (d, 2 H, J_{H-H} = 6.6, NCHC*H*), 3.99 (quint, 6 H, J_{H-P} = 6.9, J_{H-H} = 6.9, CH_2), 1.23 (t, 9 H, J_{H-H} = 6.9, CH_3)	147 (s, J_{P-W} = 384)

[a] Measured in CH_2Cl_2 solution. [b] Measured in acetone-d_6. [c] Reported in ppm relative to $\delta(Me_4Si)$ = 0 ppm. [d] Reported in ppm relative to δ(85% H_3PO_4) = 0 ppm. [e] The signals due to the AA′MM′ spin system in symmetrical Cp ligands are, due to their simple appearance, reported as triplets with coupling constants equal to half of the separation between the two outer lines. Abbreviations: s = singlet, d = doublet, quint = quintet, t = triplet, m = multiplet.

(pyridine) charge-transfer (MLCT) transitions bands fall in the range 390−600 nm, and ligand-field (LF) bands appear from 350 to 410 nm. The two different absorptions are differentiated from each other via the assistance of solvatochromism: (1) charge-transfer bands are prone to blue shift as solvent polarity increases while ligand-field bands are generally much less susceptible to such changes[25] (see Figure 1 for complex **4**); (2) a good correlation exists between MLCT absorption maxima (cm^{-1}) and the solvent parameter, E^*_{MLCT} (see Figure 2 for [$(CO)_4$(L)W]$_2$(μ-**BPEB**)). The E^*_{MLCT} values were derived by Manuta and Lees[26] from solvatochromism studies on the related (bpy)M$(CO)_4$ complexes (M = Cr, Mo, W), and they have been defined between 0.00 (isooctane) and 1.00 (dimethyl sulfoxide).

For complexes $(CO)_4$(L)W(**FPA**), an intense absorption band (>460 nm), which is well separated from the LF band and exhibits negative solvatochromism,[25] still remained unassigned. Although the effect of binucleation on the relative MLCT energies has to await an extensive study, a comparison between $(CO)_4(PEt_3)$W(η^1-**DPB**) (489 nm/CH_2Cl_2; 454 nm/acetone) and **3** (530 nm/CH_2Cl_2; 504 nm/acetone) implies that the pyridyl ligand π^* orbital is stabilized on forming the dimer complexes.

Ancillary ligands, L, have a strong influence on the MLCT energies of the complexes, and the MLCT energies are ordered in accordance with the π-accepting ability of the ligands, L = CO > $P(OR)_3$ > PPh_3 > PR_3. A stronger π-accepting ancillary ligand should lower the energy of d orbitals and thus increase the energy of the MLCT (dπ to pyridyl π^*) band. Influence of pyridyl ligands on the MLCT band is also evident (see Figure 3), and the MLCT energies for $(CO)_4$(L)W(μ-**DPB**)W$(CO)_4$(L) (**I**), $(CO)_4$(L)W(μ-**BPEB**)W$(CO)_4$(L) (**II**), $(CO)_4$(L)W(**FPA**) (**III**), $(CO)_4$(L)W(**NPPA**) (**IV**), and $(CO)_4$(L)W(**APPA**) (**V**) are ordered **V** ≈ **III** > **II** ≈ **IV** > **I**. The lower MLCT energies for $(CO)_4$(L)W(μ-**DPB**)W$(CO)_4$(L) than the corresponding $(CO)_4$(L)W(μ-**BPEB**)W$(CO)_4$(L) suggests that the diethynyl unit of the **DPB** bridge is more efficient than the 1,4-bis(ethynyl)-

(24) (a) Zulu, M. M.; Lees, A. J. *Inorg. Chem.* **1988**, *27*, 1139. (b) Lees, A. J.; Fobare, J. M.; Mattimore, E. F. *Inorg. Chem.* **1984**, *23*, 2709. (c) Gaus, P. L.; Boncella, J. M.; Rosengren, K. S.; Funk, M. O. *Inorg. Chem.* **1982**, *21*, 2174. (d) Pannel, K. H.; Gonzalez, M. G. de la P. S.; Leano, H.; Iglesias, R. *Inorg. Chem.* **1978**, *17*, 1093. (e) Wrighton, M. S.; Abrahamson, H. B.; Morse, D. L. *J. Am. Chem. Soc.* **1976**, *98*, 4105.

(25) Kaim, W.; Kuhlmann, S.; Ernst, S.; Olbrich-Deussner, B.; Bessenbacher, C.; Schulz, A. *J. Organomet. Chem.* **1987**, *321*, 215.

(26) (a) Kaim, W.; Kohlmann, S. *Inorg. Chem.* **1986**, *25*, 3306. (b) Manuta, D. M.; Lees, A. J. *Inorg. Chem.* **1983**, *22*, 3825.

Table 5. UV Spectra of Compounds and Assignments in Different Solvents and Linear Correlation Parameters with E^*_{MLCT}[a]

	λ_{max}, nm, MLCT (LF)[b]						
compd	CCl_4	benzene	CH_2Cl_2	acetone	DMSO	A, cm^{-1} [c]	B, cm^{-1} [c]
2	not soluble	451 (406)	434 (408)	o (401)	o (399)	21280	2630
3	613 (385)	575 (385 sh)	530 (o)	505 (o)	494 (o)	15810	4600
4	561 (390)	537 (400 sh)	506 (o)	481 (o)	473 (o)	17320	3890
5	527 (400)	506 (400 sh)	478 (o)	465 (o)	460 (o)	18650	3280
6	522 (385)	499 (400 sh)	478 (o)	454 (o)	446 (o)	18700	3760
7		430 sh (407)	o (402)	o (400)	o (401)		
8	532 (385 sh)	498 (395)	477 (o)	452 (0)	446 (o)	18450	4120
9	497 (385 sh)	487 (o)	448 (o)	437 (o)	429 (o)	19510	3950
10	481 (o*)	459 (o)	438 (o)	423 (o)	419 (o)	20780	3150
11	473 (385 sh)	456 (o)	440 (o)	426 (o)	418 (o)	20470	3580
13	<350 (405)	<350 (398)	<350 (392)	<350 (383)	<350 (403)		
14	<350 (o)	<350 (400 sh)	(400)[d]	<350 (410)	<350 (414)		
15	<350 (o)	<350 (410 sh)	<350 (410)	<350 (404)	<350 (398)		
16	<350 (o)	<350 (o)	<350 (o)	<350 (o)	<350 (392)		
18	438 (405)	435 sh (404)	o (400)	393 (o)	392 (o)	22190	3520
19	542 (o)	516 (400 sh)	488 (395 sh)	461 (o*)	452 (o*)	17910	4270
20	511 (407 sh)	487 (407 sh)	454 (395 sh)	439 (400 sh)	426 (o)	19030	4490
21	485 (o)	463 (o)	444 (395 sh)	427 (o)	419 (o)	20230	3690
23		360 (392)	335 (386)	387 (o*)	398 (o*)		
24e			489	454			
25e			(382)	(382)	(382)		

[a] Reference 28. [b] MLCT = tungsten dπ to pyridine π^* charge transfer; LF = tungsten ligand field transition. [c] Parameters for equation $\nu_{MLCT} = A + BE^*_{MLCT}$. [d] Overlaps substantially with LF bands of **FCEP** (350 nm, 450 nm). [e] **24** = $(CO)_4(PEt_3)W(\eta^1$-**BPB**); **25** = $W(CO)_4(PPh_3)$(piperidine). Key: sh = shoulder; o = overlaps substantially with MLCT (or LF) transition; o* = ϵ of LF transition is too low compared to that of MLCT transition.

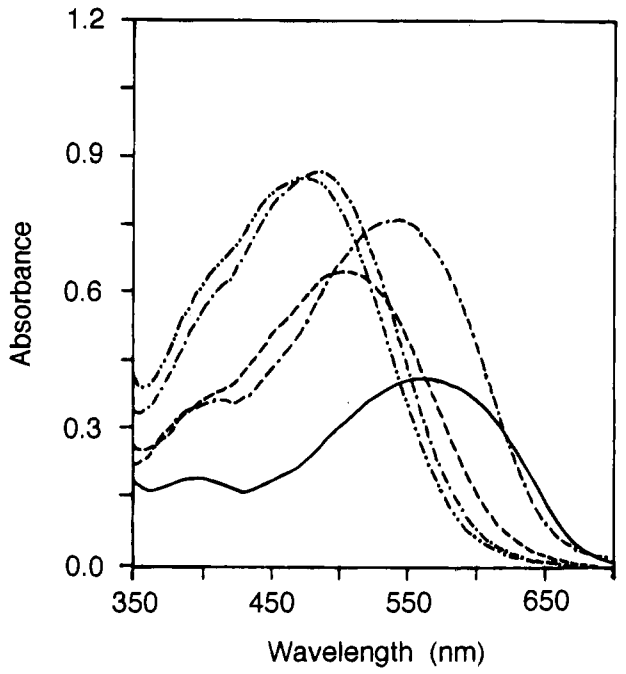

Figure 1. Electronic spectra of $[(CO)_4(PPh_3)W]_2(\mu$-**DPB**) (**4**): (—) CCl_4; (— — •) benzene; (— — —) CH_2Cl_2; (— • —) acetone; (— • •) DMSO.

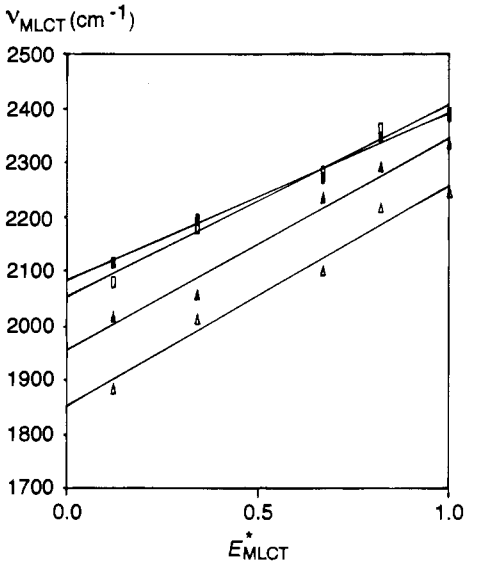

Figure 2. Metal-to-ligand charger transfer absorption maxima ν_{MLCT} of $[(CO)_4(L)W]_2(\mu$-**BPEB**), plotted against the solvent parameter E^*_{MLCT}.[28] Key: triangle; L = PMe_3; solid triangle, L = PPh_3; rectangle, L = $P(OEt)_3$; solid rectangle, L = $P(OMe)_3$.

phenyl unit of the **BPEB** bridge in stabilizing the pyridyl ligand π^* orbital. The conjugation of π-electrons in **BPEB** bridged dimers might be less efficient owing to the mismatch of a phenyl p orbital and an alkynyl p orbital in energy, a phenomenon frequently observed in nonlinear optical materials.[27] The para-substituents which have possible π interaction with the pyridine ring were found to have a great effect on the metal to pyridyl ligand charger transfer energy.[28] Accordingly, the electron-donating aminophenyl moiety and the ferrocenyl moiety[29] would raise the energy of the pyridyl ligand π^* orbital, and the electron-withdrawing *p*-nitrophenyl moiety would do the opposite. It is interesting that the energy of the metal to the pyridyl π^* charge transfer is ordered **II** $\approx$ **IV** > **I**. Whether the lowering of the energy in **I** relative to **IV** is really due to the effect of binucleation has to be scrutinized in more detail.

Electrochemistry. Redox potential values obtained from cyclic voltammetry data of the compounds in this study are listed

(27) (a) Cheng, L. T.; Tam, W.; Marder, S. R.; Stiegman, A. E.; Rikken, G.; Spangler, C. W. *J. Phys. Chem.* **1991**, *95*, 10643. (b) Stiegman, A. E.; Graham, E.; Perry, K. J.; Khundkar, L. R.; Cheng, L. T.; Perry, J. W. *J. Am. Chem. Soc.* **1991**, *113*, 7658.

(28) (a) Sutton, J. E.; Taube, H. *Inorg. Chem.* **1981**, *20*, 4021. (b) Ford, P.; Rudd, De F. P.; Gaunder, R.; Taube, H. *J. Am. Chem. Soc.* **1968**, *90*, 1187.

(29) (a) Cheng, L. T.; Tam, W.; Meredith, G. K.; Marder, S. R. *Mol. Cryst. Liq. Cryst.* **1990**, *189*, 137. (b) Green, M. L. H.; Qin, J.; O'Hare, D.; Bunting, H. E.; Thompson, M. E.; Marder, S. R.; Chatakondu, K. *Pure Appl. Chem.* **1989**, *61*, 817. (c) Green, M. L. H.; Marder, S. R.; Thompson, M. E.; Bandy, J. A.; Bloor, D.; Kolinsky, P. V.; Jones, R. J. *Nature* **1987**, *330*, 360.

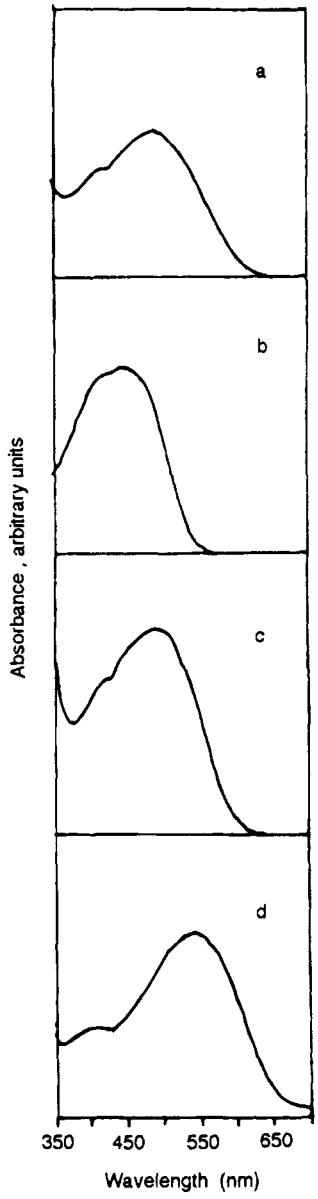

Figure 3. Electroni Pergamon Pressc spectra of $[(CO)_4(PPh_3)W]_2(\mu$-Y) in benzene at 25 °C: (a) Y = **NPPA**; (b) Y = **FPA**; (c) Y = **BPEB**; (d) Y = **DPB**.

in Table 6. Cyclic voltammograms which illustrate the effects of variation of ancillary ligands on the redox potentials are in Figure 4. All the oxidation processes are irreversible, and the oxidation potentials indicate that the HOMO levels of the homologous complexes are ordered L = CO > $P(OR)_3$ ≥ PPh_3 > PR_3. Replacement of phosphorus donor ligand for CO significantly lowers the HOMO level of the complexes by 0.3−0.4 eV, whereas perturbation on the HOMO energy is smaller upon variation of phosphorus donor ligands. On the other hand, variation of the pyridyl ligand does not appear to affect the oxidation potentials of the compounds to a significant extent.

Although the reduction potentials for the free pyridyl ligands were found to be irreversible, two reversible one-electron reduction potentials (judged from comparing the anodic peak-cathodic peak separations to that of ferrocene, see Experimental Section), $E_{red}(0/1-)$ and $E_{red}(1-/2-)$, were observed for complexes $(CO)_4(L)W(\mu$-**DPB**$)W(CO)_4(L)$ (**I**) and $(CO)_4(L)W(\mu$-**BPEB**$)W(CO)_4(L)$ (**II**) except for **3**. This observation could be attributed to the stabilization of the ligand π^* orbitals in the bridged compounds.[24a] For molecules with two chemically equivalent and reversible redox sites the difference between

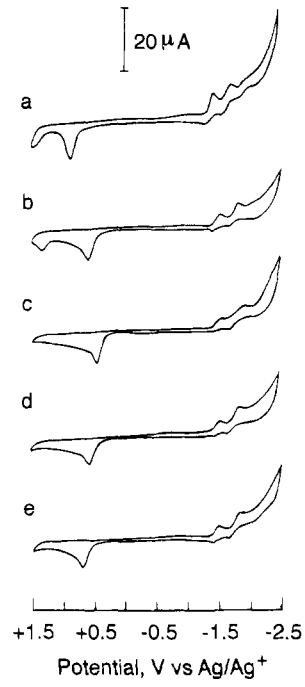

Figure 4. Cyclic voltammograms of $[(CO)_4(L)W]_2(\mu$-**DPB**) in deoxygenated CH_2Cl_2 containing 0.1 M TBAP at 25 °C: (a) L = CO; (b) L = PPh_3; (c) L = PEt_3; (d) L = $P(OEt)_3$; (e) L = $P(OPh)_3$. All potentials are in volts versus $Ag/AgNO_3$ (0.01 M in MeCN; scan rate is 80 mV s^{-1}).

these reduction potentials may be related to conproportionation (anion-radical stability) constant K_{con},[30] i.e., the degree of the energy stabilization of ligand π^*-acceptor orbital. Lees also rationalized the reduction potential differences for some dipyridyl-bridged ditungsten complexes, $[W(CO)_5]_2(\mu$-**BP**), in terms of energy repulsion between the two electrons in the highest occupied antibonding orbital of $[W(CO)_5]_2(\mu$-**BP**$)^{2-}$, and suggested that the repulsion energy decreased as the distance between the $W(CO)_5$ fragments increased.[24a] The reduction potential differences in **I** (0.28−0.35 V) and **II** (0.23−0.30 V) appear to be not very sensitive to the variation of either ancillary ligands or the bridging ligands, and are also similar to that (0.26 V) reported for $[(CO)_5W]_2(\mu$-bpe) (bpe = *trans*-1,2-bis(4-pyridyl)ethylene).[24a] We suspect that the repulsion energy is not simply due to the difference between the two metal fragments. The E_{red} values of $(CO)_4(L)W($**FPA**$)$ appear to be much higher than those in **I** and **II**, suggesting the higher pyridyl π^* orbital energy. We are not able to rationalize E_{red} values for $(CO)_4(L)W($**NPPA**$)$ due to the presence of the two redox values involving the free **NPPA**.

The potential difference (E_p) between the oxidation and the reduction potentials, $E_{ox} - E_{red}(0/1-)$, seems to be in agreement with the MLCT transition energy: (1) within the same series (e.g., **I**, **II**, **III**, or **IV**) of complexes, the E_p values are ordered L = CO > $P(OR)_3$ ≈ PPh_3 > PR_3; (2) for the same ancillary ligand, the E_p values are ordered **III** > **II** > **I**.

Molecular Structure of $[(CO)_4(P(OPh)_3)W]_2(\mu$-DPB) (6), $[(CO)_4(P(OMe)_3)W]_2(\mu$-BPEB) (10), $(CO)_4(P(OEt)_3)W($FPA) (16), and $(CO)_4(PEt_3)W($NPPA) (19). The ORTEP drawings of **6**, **10**, **16**, **and 19** are shown in Figures 5−8, respectively. The tungsten atom resides in an approximately octahedral environment and the pyridyl ligand is cis to the phosphite or phosphine ligand. The d_{xz} and d_{yz} orbitals are expected to effectively participate in the metal to pyridyl π^* charge transfer (the N−W−C_3 is taken to be the z axis) if the dihedral angle

(30) Haga, M. A.; Koizumi, K. *Inorg. Chim. Acta* **1985**, *104*, 47.

Table 6. Redox Potentials for Complexes in CH_2Cl_2 at 298 K[a]

complex				
no.	formula	E_{ox}	E_{ox}[b]	E_{red} (ΔE_p)[c]
2	$(OC)_5W$(**DPB**)$W(CO)_5$	+0.64 (i)		−1.59 (105), −1.87 (112)
3	$(OC)_4(PEt_3)W$(**DPB**)$W(CO)_4(PEt_3)$	+0.25 (i)		−1.67 (115), −2.02 (170)
4	$(OC)_4(PPh_3)W$(**DPB**)$W(CO)_4(PPh_3)$	+0.37 (i)		−1.67 (103), −1.98 (105)
5	$(OC)_4(P(OEt)_3)W$(**DPB**)$W(CO)_4(P(OEt)_3)$	+0.34 (i)		−1.69 (95), −1.99 (110)
6	$(OC)_4(P(OPh)_3)W$(**DPB**)$W(CO)_4(P(OPh)_3)$	+0.48 (i)		−1.67 (113), −1.99 (118)
7	$(OC)_5W$(**BPEB**)$W(CO)_5$	+0.66 (i)		−1.93 (92), −2.23 (130)
8	$(OC)_4(PMe_3)W$(**BPEB**)$W(CO)_4(PMe_3)$	+0.22 (i)		−1.97 (95), −2.22 (110)
9	$(OC)_4(PPh_3)W$(**BPEB**)$W(CO)_4(PPh_3)$	+0.33 (i)		−2.00 (95), −2.23 (93)
10	$(OC)_4(P(OMe)_3)W$(**BPEB**)$W(CO)_4(P(OMe)_3)$	+0.35 (i)		−1.98 (105), −2.24 (100)
11	$(OC)_4(P(OEt)_3)W$(**BPEB**)$W(CO)_4(P(OEt)_3)$	+0.33 (i)		−2.00 (99), −2.24 (102)
13	$(OC)_5W$(**FPA**)	+0.65 (i)	+0.76 (i); +0.26	−2.29 (i)
14	$(OC)_4(PEt_3)W$(**FPA**)	+0.28 (i)	+0.26 (i); +0.26	−2.46 (i)
15	$(OC)_4(PPh_3)W$(**FPA**)	+0.32 (i)	+0.37 (i); +0.24	−2.49 (i)
16	$(OC)_4(P(OEt)_3)W$(**FPA**)	+0.31 (i)	+0.40 (i); +0.23	−2.49 (i)
18	$(OC)_5W$(**NPPA**)	+0.66 (i)		−1.46 (100), −1.84 (80)
19	$(OC)_4(PEt_3)W$(**NPPA**)	+0.23 (i)		−1.46 (99), −1.87 (108)
20	$(OC)_4(PPh_3)W$(**NPPA**)	+0.34 (i)		−1.46 (112), −1.89 (86)
21	$(OC)_4(P(OEt)_3)W$(**NPPA**)	+0.33 (i)		−1.47 (104), −1.91 (115)
23	$(OC)_5W$(**APPA**)	+0.69 (i)		−1.53 (i), −2.24, −2.71 (i)
DPB				−2.22 (i), −2.37 (i)
BPEB				−2.39 (i)
FPA				>−2.89
NPPA				−1.42 (100), −2.12 (205)
APPA		+1.09 (i)		−1.43 (i), −2.01 (i), −2.21 (i)

[a] Analyses performed in 10^{-3} M deoxygenated CH_2Cl_2 solutions containing 0.1 M TBAP, scan rate is 80 mV. All potentials in volts vs ferrocene (0.00 v with peak separation of 105 mV in CH_2Cl_2); scan range +1.5 to −2.5 V; i = irreversible process. [b] The measurements were taken in CH_3CN since the oxidation peak for tungsten is almost merged in the reversible peak of Fe(+2/+3) when the measurements were taken in CH_2Cl_2. [c] $\Delta E_p = E_{pa} - E_{pc}$, mV.

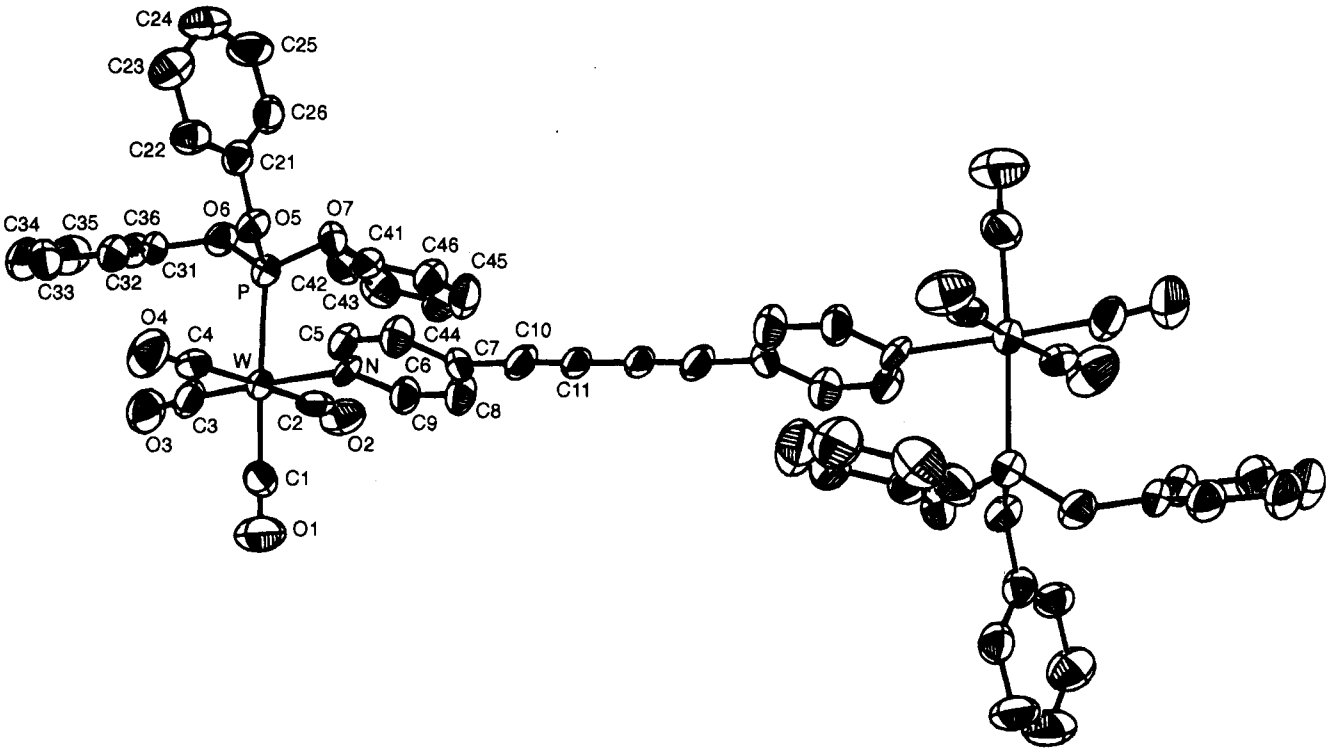

Figure 5. ORTEP drawing of $[(CO)_4(P(OPh)_3)W]_2(\mu$-**DPB**) (**6**). Thermal ellipsoids are drawn with 30% probability boundaries.

between the pyridyl ring and the best plane consisting of W, N, C2, C3, and C4 are 0, 45, or 90°. The conformer with the dihedral angle of 90° is likely to be least favored because of the better π-accepting of CO than phosphine (phosphite) as well as the steric repulsion between the ortho hydrogen atoms and the substituents on the phosphorus atom. Comparison of the strength of MLCT based on the solid state structure is currently not available due to different extents of deviation of the pyridyl ring (plane A) and the W/N/C2/C3/C4 plane (plane B) from coplanarity for **6** (the largest deviations of atoms from the least-squares planes A and B are 0.00(2) Å and 0.05(2) Å, respectively; dihedral angle = 18.0(4)°), **10** (the largest deviations of atoms from the least-squares planes A and B are 0.01(1) and 0.07(2) Å, respectively; dihedral angle = 4.1(3)°), **16** (the largest deviations of atoms from the least-squares planes A and B are 0.02(3) and 0.04(3) Å, respectively; dihedral angle = 18.7(7)°), and **19** (the largest deviations of atoms from the least-squares planes A and B are 0.02(2) and 0.08(2) Å,

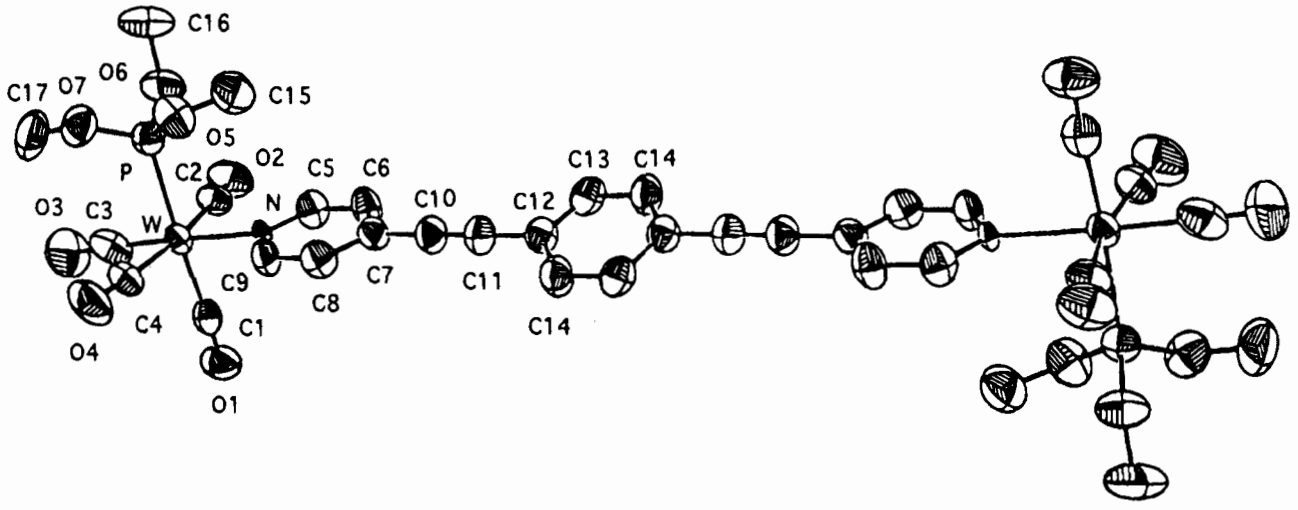

Figure 6. ORTEP drawing of $[(CO)_4(P(OMe)_3)W]_2(\mu$-**BPEB**) (**10**). Thermal ellipsoids are drawn with 30% probability boundaries.

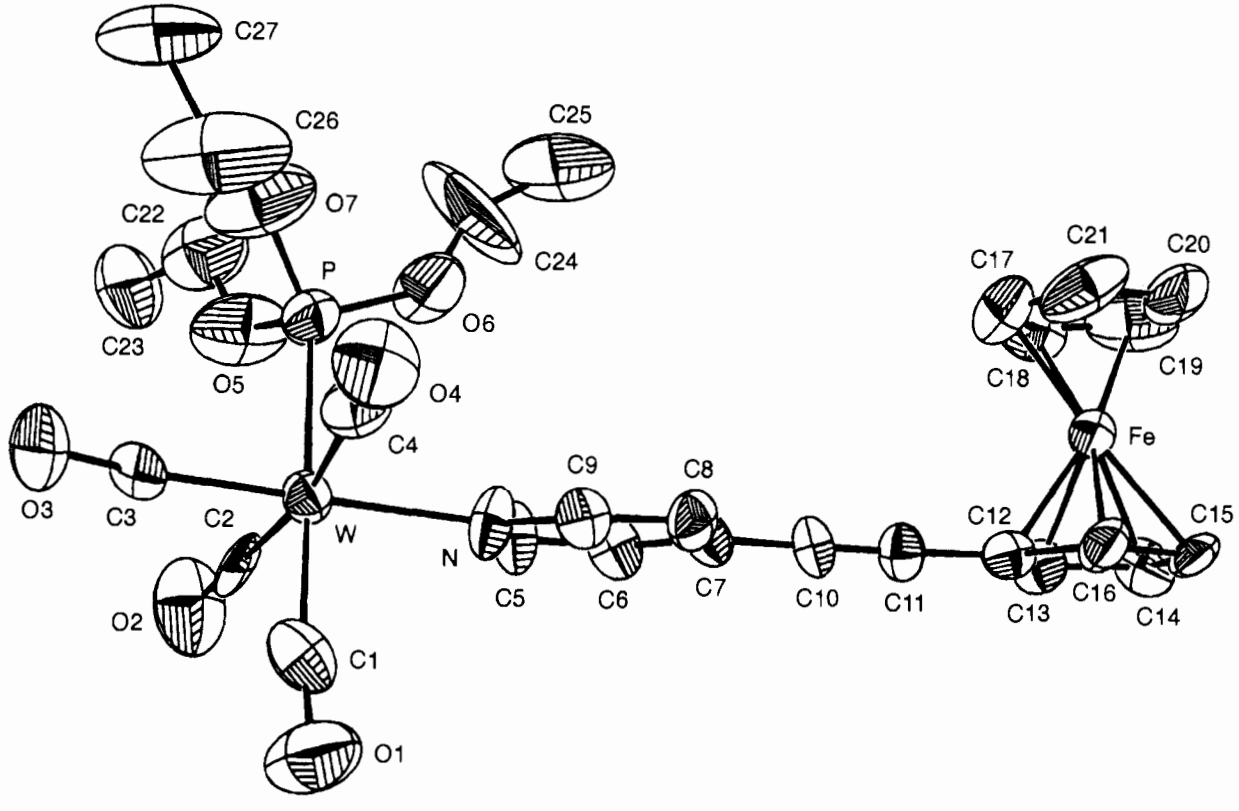

Figure 7. ORTEP drawing of $(CO)_4(P(OEt)_3)W$(**FPA**) (**16**). Thermal ellipsoids are drawn with 30% probability boundaries.

respectively; dihedral angle = 32.9(5)°). Retainment of the planarity of the backbone in the bridge is regarded to be important for conjugation of π electrons through the bridge. Although the aromatic rings (Py, Cp, Ph) on the bridge in **6** and **16** are found to be coplanar, deviation of the aromatic rings from coplanarity is found to occur in **10** (dihedral angle between successive py and Ph rings is 16.7(5)°; the largest deviations of atoms from the least-squares planes are 0.01(1) and 0.00(3) Å for py and Ph rings, respectively) and in **19** (dihedral angles of py/Ph and Ph/NO_2 are 9.1(5) and 5.8(8)°, respectively; the largest deviations of atoms from the least-squares planes are 0.02(2), 0.01(2), and 0.00(3) Å for py, Ph, and NO_2, respectively). Therefore, information on effectiveness of the delocalization of the metal to ligand charge transfer through the bridge was also elusive from the solid state structural data. Charge transfer was reported to result in the quinonoid character, bond alternation of the aromatic ring, of approximately planar and fully extended organic compounds $NH_2C_6H_4(C{\equiv}C)_nC_6H_4NO_2$ (n = 0−3).[31] We were not able to observe such a bond alternation in the pyridyl ring in all four complexes, or nitrophenyl in **19** because of large esd's for the bond distances and angles.

The W−C−O linkage (173(2)−178(1)°) does not deviate significantely from linearity. The carbonyl W−C distances range from 1.88(2) to 2.03(2) Å, and the two mutual cis carbonyl ligands have slightly longer W−C distances, as expected. Other relevant crystal data also appear to be normal: the W−P distances range from 2.437(3) to 2.529(4)°; the alkynyl C≡C distances range from 1.14(2) to 1.19(1) Å. The W−N distances (2.255(7)−2.29(1) Å) are also comparable to literature values.[32]

(31) Graham, E. M.; Miskowski, V. M.; Perry, J. W.; Coulter, D. R.; Stiegman, A. E.; Schaefer, W. P.; Marsh, R. E. *J. Am. Chem. Soc.* **1989**, *111*, 8771.

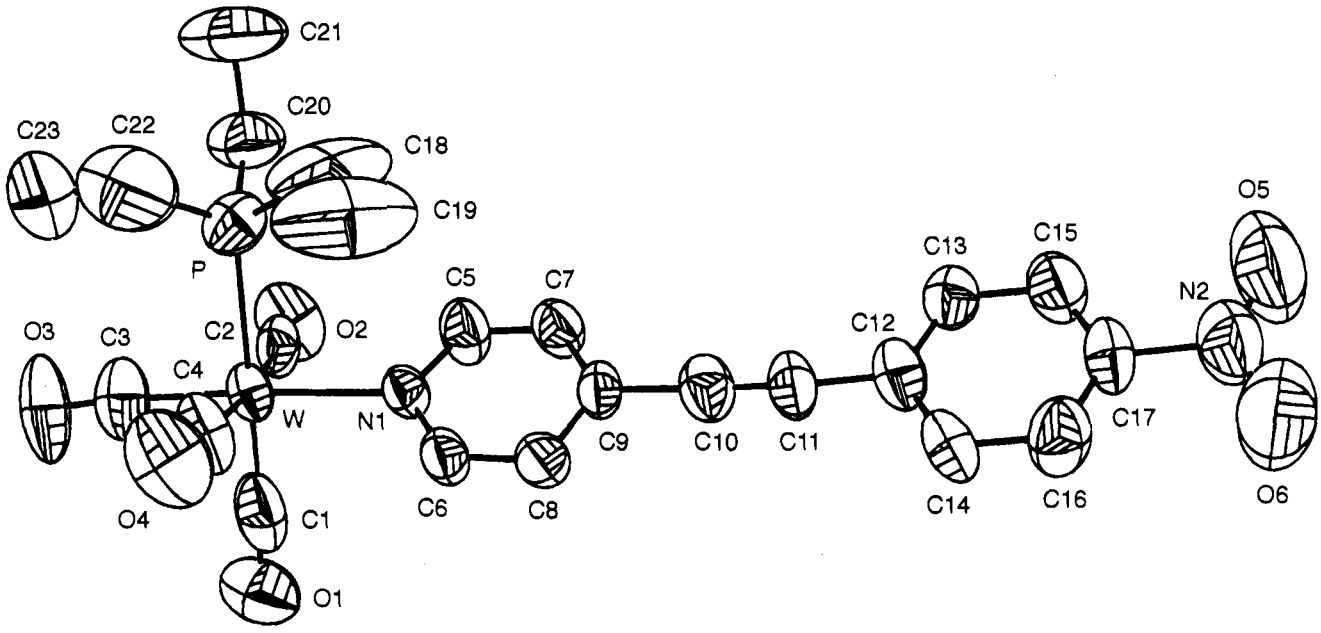

Figure 8. ORTEP drawing of $(CO)_4(PEt_3)W$(**NPPA**) (**19**). Thermal ellipsoids are drawn with 30% probability boundaries.

Conclusion

Several series of metal complexes of ethynyl pyridyl ligands were synthesized. Through optical spectroscopy and electrochemical analysis we have demonstrated that variation of ancillary ligands as well as the ethynyl pyridyl ligands could potentially allow one to design suitable molecules for electron transfer studies and nonlinear optical studies. Variation of metal atoms is also included in our future studies.

Acknowledgment. We thank the National Science Foundation of the Republic of China for financial support (Grants NSC-83-0208-M-001-100 and NSC-84-2113-M-001-017).

Supplementary Material Available: Tables of complete crystal data, all bond distances and angles, anisotropic thermal parameters and isotropic thermal parameters, positional parameters for calculated hydrogen atoms, and dihedral angles between the least-squares planes and stereoviews for complexes **6**, **10**, **16**, and **19** (28 pages). Ordering information is given on any current masthead page.

IC941248Q

(32) Lin, J. T.; Huang, P. S.; Tsai, T. Y. R.; Liao, C. Y.; Tseng, L. H.; Wen, Y. S.; Shi, F. K. *Inorg. Chem.* **1992**, *31*, 4444.